Comparison of Measured and Calculated Vibrations of a Turbocharger

<u>Andreas Fuchs</u> [1], Thomas Klimpel [2], Joachim Schmied [1], Karl-Heinz Rohne [2]

[1] Delta JS AG, Technoparkstr. 1, CH-8005 Zürich, Switzerland, {afuchs}, {jschmied}@delta-js.ch
[2] ABB Turbo Systems AG, Bruggerstr. 71a, CH-5401 Baden, Switzerland, {thomas.klimpel},
{karl-heinz.rohne}@ch.abb.com

Abstract

Exhaust gas turbochargers are usually rotor – bearing – systems with high circumferential speed, rather small weight and therefore small static bearing loads. These rotors are typically mounted in floating or semi floating ring bearings. Such bearings have an inner and an outer oil film, which are coupled hydraulically, energetically and by the forces arising from each oil film. The 2D oil film pressure, the 3D temperature distribution in the oil film, in the floating ring and in the bearing shell, the linear static and dynamic bearing coefficients as well as the nonlinear load capacity and the nonlinear damping behaviour can be more precisely calculated with the enhanced program ALP3T2Penhanced (considering two phase model and inertia forces in the oil film) compared to classical cavitation models such as Gümbel and Reynolds boundary conditions. The calculation is based on an iterative solution of the extended Reynolds, energy and deformation equations, including temperature and pressure dependent properties of the oil film.

In the present case a turbocharger supported on non-centred semi-floating ring bearings is analysed with MADYN 2000, which includes the program ALP3T2Penhanced. To efficiently calculate the speed dependent bearing characteristics including speed dependent temperatures and clearance changes an approach with some simplifications according to DIN is applied.

The behaviour of such turbochargers is highly nonlinear, since the outer film, which acts as a squeeze film, can only create a load carrying force by vibration. Thus the calculation must consider the nonlinear bearing forces. The centring effect is shown as well as the sub-synchronous and synchronous response.

The results for several variants with different unbalances, clearances and inlet temperatures are compared to measurements. The resulting synchronous as well as non-synchronous vibrations agree well with the measurements. This proves, that the simplifications, which were used in order to allow an efficient analysis, did not compromise the quality of model.

Nomenclature

B	bearing width	u,v,w	flow velocities $u=U/(\Omega r), v=V/(\Omega\Delta R), w=W/(\Omega r)$
c	lubricant specific heat	α_D	resulting angle of bearing pressure
d_{ik}	damping coefficient	ΔR	radial bearing clearance $R-r$
D	bearing diameter $2R$	γ	attitude angle of journal
H	dimensionless film thickness $h/\Delta R$	ε	relative eccentricity of journal $e/\Delta R$
K_x, K_z	turbulence factors	$\varepsilon_{h,v}$	horizontal, vertical canting of journal $\varepsilon_i=(x,y)/\Delta R$
m	mass	η	lubricant dynamic viscosity
p	pressure	φ	angular coordinate
r	journal radius	ϕ	dimensionless time Ωt
R	journal bearing radius (inside)	Π	dimensionless lubricant pressure $p\psi^2/(\eta\Omega)$
R_S	pad radius	ρ	density
Re	Reynold number Re$=\rho\Omega r\Delta R/\eta$	ψ	relative bearing clearance $\Delta R/R$
Re*	modified Reynolds number Reψ	ψ_S	relative pad clearance $(R_S-r)/\Delta R$
So_D	Sommerfeld number for rotation $F_{stat}\psi^2/(BD\eta\Omega)$	τ	centre angle of pad radius
T	temperature	Ω	journal rotational velocity
V	volume of phase	ω	journal vibration frequency
$\bar{y}, \bar{z}$	radial, axial coordinate $\bar{y}=y/\Delta R, \bar{z}=z/r$		

1 Introduction

For the calculation of simple bearings, floating and semi-floating ring bearings normally only insufficient models are used for the energy coupling of the lubricating oil film in circumferential, axial and radial direction [1] – [3]. For floating ring bearings and squeeze film dampers, the energetically coupling of the oil films by the radial heat conduction and oil flow is in general neglected or only considered by rough approaches [4]. These effects can considerably influence the transient bearing capacity and thus the allowable unbalance, the threshold of self-excited vibrations and the load capacity of squeeze film dampers for high velocities.

Therefore an efficient method is presented for calculating the stationary and transient load capacity of general radial journal bearings, floating ring bearings and squeeze film dampers, which takes into account the important "additional effects" for high vibration velocities. By integrating the journal bearing program into a linear and non-linear rotor-dynamic program [5], complex rotor bearing systems can be also calculated for difficult operating conditions.

2 Theory

High friction losses occur in the oil film for high sliding velocities due to the viscosity of the oil. This yields high temperature gradients in the lubricating film due to the low heat conductivity of typically used oil types. Therefore extended formulas of the basic equations have to be used for calculating the hydrodynamic pressure and temperature distribution in high-speed journal bearings. These formulas must consider the change of the strongly temperature-dependent viscosity of the lubricating oil in all three coordinate directions [3]. Solving the energy equation and the appropriate heat transfer equations leads to three-dimensional temperature distribution of the lubricating film, the bearing bush and the shaft.

Significant simplifications are used in the calculation procedures in [3] in contrast to ALP3T2Penhanced, such as idealized geometry of the bearings, negligence of the thermal and elastic deformations of the bearing bush, symmetrical boundary conditions in axial direction for the calculation of the pressure and temperature distribution, and negligence of the local inertia forces in the lubricating film.

The local film thickness of each lobe or pad can be described by equation (1), see [6]

$$H(\varphi,\bar{z}) = \underbrace{\frac{\psi_S}{\psi} + \left(\frac{\psi_S}{\psi}-1\right)\cos(\varphi-\tau)}_{\text{curvature of lobe or pad}} + \underbrace{\frac{\delta}{\psi}(1+\psi_d)\sin(\varphi-\tau)+H_K}_{\text{tilting and deflection of pad}} \underbrace{-\,\varepsilon\cos(\varphi-\gamma)}_{\substack{\text{displacement}\\\text{of shaft}}} \underbrace{-\bar{z}\frac{\sqrt{\varepsilon_h^2+\varepsilon_v^2}}{B/D}\cos\left(\varphi-\arctan\frac{\varepsilon_h}{\varepsilon_v}\right)}_{\text{misalignment}}. \quad (1)$$

2.1 Two Phase Model for Lubricating Film

It is possible to capture the influence of the air, which is dissolved in the lubricating oil, and the mixture of air and oil in the cavitation area with a quite simple two-phase flow model. As it is shown by several studies, the air which is solved in the oil does not change the viscosity and the density of the oil very much [8]. In contrast, the viscosity of the oil-air mixture changes noticeably for increasing foaming of the lubricating film. The variation of the viscosity due to the air-oil mixture depends on the diameter and surface tension of the air bubbles and the shear stress in the lubricating gap [8]. In hydrodynamic bearings and squeeze film dampers the following approach can be derived, since the shear stress is usually much bigger than the surface tension of the air bubbles:

$$\eta_{mix} = \eta_{Oil}(1-C) = \eta_{Oil}\frac{V_{total}-V_b}{V_{total}} = \eta_{Oil}\frac{1}{1+r}, \quad (2)$$

with $C = V_b/V_{total} = V_b/(V_b+V_{oil})$ degree of foaming, $r = V_b/V_{Oil}$ factor for the amount of bubbles.

The relative local density ρ_{mix} depends on the gas diffusing in and out of the oil. It is modelled as a function of the film pressure. The undissolved air arises as bubbles in the oil. The ratio r between the undissolved gas and the oil can be calculated by use of the Henry-Daltons and Boyle-Mariottes law:

$$r = r_0\frac{T\,p_0}{T_0\,p} - a_v\frac{T_0\,p-p_0\,T}{T_0\,p}, \quad (3)$$

with p = absolute pressure, T = absolute temperature in Kelvin and index 0 for ambient conditions. By neglecting the mass of the undissolved air the relative local density is:

$$\rho_{mix} = \frac{m_{Oil}+m_b}{V_{Oil}+V_b} \approx \rho_{Oil}\frac{1}{1+r}. \quad (4)$$

The Bunsen-Coefficient is $a_v \approx 0.08 \dots 0.09$ for relevant mineral oils (ISO-VG 32 to ISO-VG 220) and is nearly independent of the temperature (T = 20 °C to 100 °C) [9].

2.2 Pressure Distribution in the bearing

The flow can be described in journal bearings and squeeze film dampers by using the following extended Reynolds equation which includes also the inertia forces of the oil film [6]:

$$\frac{\partial}{\partial \varphi}\left(\frac{H^3}{12\eta_P^* K_x}\frac{\partial \Pi}{\partial \varphi}\right) + \frac{\partial}{\partial \bar{z}}\left(\frac{H^3}{12\eta_P^* K_x}\frac{\partial \Pi}{\partial \bar{z}}\right) = \frac{1}{2}\frac{\partial(\rho_{mix} f_C H)}{\partial \varphi} + \frac{\partial(\rho_{mix} H)}{\partial \phi} + R_1(\varphi,\bar{z}) + R_2(\varphi,\bar{z},\phi),$$

$$R_1 = -\mathrm{Re}^*\left\{\frac{\partial}{\partial \varphi}\left[\frac{H^2}{12\eta_P^* K_x}\left(\frac{\partial}{\partial \varphi}\int_0^H \rho_{mix} u^2 d\bar{y} + \frac{\partial}{\partial \bar{z}}\int_0^H \rho_{mix} uw d\bar{y}\right)\right] + \frac{\partial}{\partial \bar{z}}\left[\frac{H^2}{12\eta_P^* K_z}\left(\frac{\partial}{\partial \varphi}\int_0^H \rho_{mix} uw d\bar{y} + \frac{\partial}{\partial \bar{z}}\int_0^H \rho_{mix} w^2 d\bar{y}\right)\right]\right\} \quad (5)$$

$$R_2 = \mathrm{Re}^*\left\{\frac{H^2}{12\eta_P^*}\frac{\partial^2 H}{\partial \phi^2} - \frac{\partial}{\partial \phi}\int_0^H \rho_{mix} u d\bar{y}\frac{\partial}{\partial \varphi}\left(\frac{H^2}{12\eta_P^*}\right) - \frac{\partial}{\partial \phi}\int_0^H \rho_{mix} w d\bar{y}\frac{\partial}{\partial \bar{z}}\left(\frac{H^2}{12\eta_P^*}\right)\right\}$$

$R_1(\varphi,\bar{z})$ represents the convective inertia forces, while $R_2(\varphi,\bar{z},\phi)$ describes the local inertia forces due to acceleration. The factors η_P^* and f_C includes the local distribution (mean values for Poiseuille and Couette-Flow, respectively) of the viscosity. These factors change in circumferential and axial direction. The local turbulent flow regime is included in equation (5) by the factors K_x and K_z. Turbulent flow occurs, if the local Reynolds number $\mathrm{Re}_l = \rho_{mix} r \Omega H / \eta$ is bigger than the critical Reynolds number Re_{cr}. The factors K_x and K_z can be calculated by using empirical equations [3].

By taking the oil foaming and the local inertia forces into account the pure Poiseuille flow remains nearly unchanged in the Reynolds equation (5) in comparison to [3], while the Couette flow will be changed and additional source terms occur for the pressure generation in the lubricating film. These effects are not included in the simple DIN calculation [2], for example.

For solving the Reynolds equation, the pressure at the edges of the pads is set to the ambient pressure Π_0 or to the pressure of the hydrostatic pocket Π_T. Additional boundary conditions at the beginning or the end of the cavitation area are not necessary in the model shown here. The pocket pressure Π_T can be calculated by means of the law of mass conservation with applied flow factors for the oil supply and resistance factors of the pocket. The resistance factor R_T of the pocket is the sum of a viscosity and density proportional resistance $R_T = R_{\eta T} + R_{\rho T}$. The Reynolds equation is solved together with the boundary conditions, the equations for the mass balance, for the fluid flow, for the local film thickness and the correction factor for turbulent flow using a finite volume method solving with an improved SLOR-solver [3], [6]. The two-dimensional pressure distribution $\Pi(\varphi,\bar{z})$ is the result of the numerical solution for the steady state part of the Reynolds equation.

2.3 Temperature Distribution in the bearing

The steady state, 3D temperature distribution $T(\varphi, y, \bar{z})$ can be calculated in the lubricating gap by solving the energy equation for compressible flow:

$$\mathrm{div}(\rho c \vec{u} T) = \mathrm{div}(\lambda \,\mathrm{grad}\, T) + \eta \Phi, \quad \Phi = \left(\frac{\partial u}{\partial y}\right)^2 + \left(\frac{\partial w}{\partial y}\right)^2. \quad (6)$$

Here, the dissipation Φ is reduced to the most dominant velocity gradients. The approach of Falz [11] is used for calculating the viscosity η as a function of the temperature ($\eta/\eta_0 = (T/T_0)^{-l}$). The turbulent flow regime is also included by the increased heat conductivity and the eddy viscosity of the oil film.

The Reynolds (5) and the energy equation (6) are nonlinearly-coupled by the physical properties of the oil (viscosity and density). Therefore both equations must be solved simultaneously in an iteration process [6]. The hot-cold-oil mixing in the pockets and the heat conductivity and transfer equations (for the bearing bush, the shaft and the environment, respectively) must also be considered. The 2D or 3D heat conductivity equations are used for the calculation of the temperature distribution in the bearing bush and in the shaft, respectively:

$$
\begin{aligned}
\text{for the bearing bush} \quad & \Delta T_B(\varphi, z, r) = 0 \\
\text{for the shaft} \quad & \Delta T_S(z, r) = 0
\end{aligned}
\qquad \Delta : \text{Laplace operator} \qquad (7)
$$

2.4 Bearing Characteristics

The static bearing properties, such as bearing load, power loss or oil flow, can be calculated by integration of the corresponding pressure distribution, the shear stress and velocity distribution, respectively, on their corresponding surfaces, if the bearing profile $H(\varphi, \bar{z}), B/D)$, the displacement of the shaft (ε, γ) and additional parameter (T_{en}, p_{en}, η_{en}, K_B, ρ, λ, α, ...) are given.

For calculating the static properties of the inner oil film the simplified DIN-model is used. That means the viscosity in the oil film is constant, the turbulence is neglected, the heat conduction of the shaft and the bearing shell is infinite compared to that of the oil, thus, the heat transfer to the environment is neglected. All the calculated bearing characteristics are only a function of the Sommerfeld number So_D. These Sommerfeld similarity can be used in order to calculate easily the temperatures of shaft, ring and bearing and the corresponding deformations later with an effective method. Also the two-phase-model is neglected in the DIN-calculation, but it is taken into account to calculate the non-linear transient bearing forces.

The transient bearing forces have to be nonlinearly calculated for high vibration amplitudes or squeeze-film dampers. In the here presented calculation method for calculating the transient bearing forces, the additional effects, which cause long computation times, are only taken into account by averaging. The transient bearing forces are split into two parts, which are proportional to the rotation and lateral movements. The bearing force corresponds to the static bearing force $[So_D, \alpha_D]$. The damping force depends linearly on the shaft moving velocity (ε', γ) according to the journal bearing theory [3] and it can be described by the use of the damping coefficients β_{ik}^*. The coefficients depend in a highly nonlinear way on the actual position of the shaft (ε, γ) in the bearing, as well as on the bearing force $[So_D, \alpha_D]$. For a squeeze film damper the static bearing force So_D is zero, which means the damper cannot produce any restoring force unless special designs are applied. Therefore squeeze film dampers or semi-floating ring bearings can only produce a restoring force, if the shaft or the ring is moving or vibrating, respectively.

$$\begin{bmatrix} \overline{\Pi}_x \\ \overline{\Pi}_y \end{bmatrix} = \begin{bmatrix} So_D \sin \alpha_D \\ So_D \cos \alpha_D \end{bmatrix}_{\varepsilon, \gamma} + \begin{bmatrix} \beta_{11}^* & \beta_{12}^* \\ \beta_{21}^* & \beta_{22}^* \end{bmatrix}_{\varepsilon, \gamma} \begin{bmatrix} X' \\ Y' \end{bmatrix}. \tag{8}$$

The damping coefficients are based on a perturbation of the extended generalized Reynolds equation (5) with the assumption that shaft experiences velocities (X', Y') around the actual shaft position. Therefore the inertia forces are neglected, as the modified Reynolds number Re^* remains small.

The perturbed variables are the pressure Π and the lubricating gap H, while the density and the temperature are not disturbed.

$$\frac{\partial H(\varphi, \bar{z})}{\partial \phi} = -X' \cdot \sin \varphi - Y' \cdot \cos \varphi, \qquad ' = \frac{\partial}{\partial \phi} = \frac{\partial}{\partial \Omega t}$$

$$\Pi(\varphi, \bar{z}) = \Pi_{stat}(\varphi, \bar{z}) + \left(\frac{\partial \Pi}{\partial X'}\right)_{stat} X' + \left(\frac{\partial \Pi}{\partial Y'}\right)_{stat} Y' \tag{9}$$

Substituting these expression in equation (6) and sorting the terms according to the first perturbation order (X', Y') yields

$$\frac{\partial}{\partial \varphi}\left[\frac{H_{stat}^3}{12\eta_P^* K_x} \frac{\partial}{\partial \varphi}\left(\frac{\partial \Pi}{\partial X'}\right)_{stat}\right] + \frac{\partial}{\partial \bar{z}}\left[\frac{H_{stat}^3}{12\eta_P^* K_z} \frac{\partial}{\partial \bar{z}}\left(\frac{\partial \Pi}{\partial X'}\right)_{stat}\right] = -\rho_{mix} \cdot \sin \varphi,$$

$$\frac{\partial}{\partial \varphi}\left[\frac{H_{stat}^3}{12\eta_P^* K_x} \frac{\partial}{\partial \varphi}\left(\frac{\partial \Pi}{\partial Y'}\right)_{stat}\right] + \frac{\partial}{\partial \bar{z}}\left[\frac{H_{stat}^3}{12\eta_P^* K_z} \frac{\partial}{\partial \bar{z}}\left(\frac{\partial \Pi}{\partial Y'}\right)_{stat}\right] = -\rho_{mix} \cdot \cos \varphi. \tag{10}$$

All implicit dependencies of other parameters and boundary conditions have to be linearized for the solution of these two perturbation equations as well. This requires the application of an iterative numerical solution procedure. Due to the two-phase model, no additional boundary conditions are necessary at the beginning and the end of the cavitation areas. The four damping coefficients ($\omega d_{ik} = \beta_{ik}^* (2B\eta\Omega)/\psi^3$) can be calculated by integration of the pressure coefficients $\partial \Pi / \partial q_n$ over the whole bearing surface:

$$\beta_{ik}^* = \frac{1}{4\frac{B}{D}} \int_0^{2\pi} \int_{-B/D}^{B/D} \left(\frac{\partial \Pi}{\partial q_k}\right) ((i-1) \cos \varphi - (i-2) \sin \varphi) \mathrm{d}\bar{z}\, \mathrm{d}\varphi \tag{11}$$

with $i, k = 1, 2$ and $q_n = X', Y'$ for n = 1, 2. The dynamic bearing coefficients β_{ik}^* depend mainly on the actual position of the shaft (ε, γ), the bearing profile, the function or the film-thickness and the bearing width ratio. For

squeeze film dampers, they depend also highly nonlinear on the vibration velocity and direction $(\dot{\varepsilon}, \dot{\gamma})$, if the two-phase-model is taken into account.

For the calculation of the bearing coefficients (So_D, α_D, β_{ik}^*) with the program ALP3T2Penhanced, necessary inputs are the bearing geometry, oil parameters, temperature and pressure boundary conditions, material parameters as well as parameters for the two-phase model. The coefficients are tabulated as a function of the shaft displacement (ε, γ) for the whole range of possible shaft positions in the bearing.

For a squeeze film damper, the "rotating speed" is $\Omega=0$. By multiplication of equation (5) with Ω/ω, setting $\Omega=0$ and neglecting the inertia forces, only the term $\partial(\rho_{mix}H)/\partial\phi$ remains on the right side of (5). In addition ω is used instead of Ω to get the dimensionless variables Π and ϕ, and there is no turbulent flow regime in the squeeze film damper. After perturbing equation (5) with equation (9) only the last 2 terms on the right hand side of equation (9) remained. In other words the squeeze film damper has only transient forces which are proportional to the vibration velocity and does not create any static force or stiffness unless certain design measures are taken for centring the squeeze ring.

The damping coefficients β_{22}^* calculated with the program ALP3T2Penhanced (squeeze film damper with 2 phase model) are compared to the limit values for the 2π-film (Sommerfeld boundary condition) and the π-film (Gümbel boundary condition) in Figure 1. The eccentricity velocity ε' becomes an additional parameter for the pure squeezing movement ($\Omega=0, \gamma'=0$) if the oil foaming is considered. It determines the cavitation in the squeeze film damper. The calculated β_{22}^*-values range between the asymptotical limit values of the π- and 2π-film for a cylindrical 360° squeeze film damper with axial oil supply. The differences between the β_{22}^*-values depend strongly on the eccentricity ε of the squeeze film damper for the three calculation models.

The influence of the cavitation is very important for small eccentricities ε, i.e. especially for high speed journal bearings with low load or statically centred squeeze film dampers. For statically non-centred squeeze film dampers, the influence of the cavitation is for all eccentricities very important, as the damping coefficients are a function of the velocity and the direction of the moving ring.
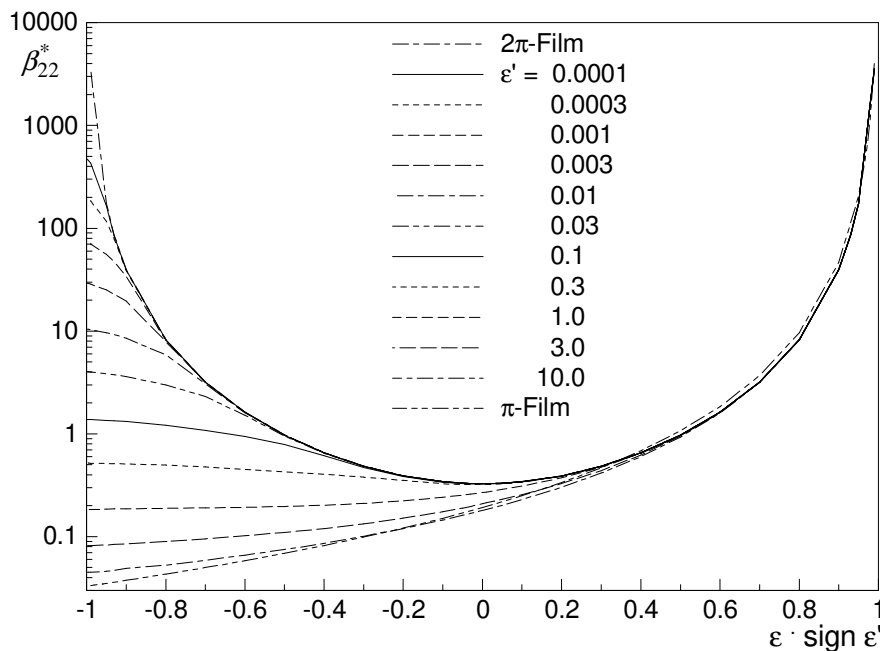
Figure 1: Comparison of the calculated Sommerfeld numbers $So_V(\varepsilon,\varepsilon')$
with Sommerfeld (2π-Film) and Gümbel (π-Film) boundary condition

The program ALP3T2Penhanced is integrated in MADYN 2000 for nonlinear calculations, which become necessary among others for high unbalances. In Figure 2 the trajectories are plotted as a verification example for a simple shaft supported in two identical 3-pad tilting pad bearings subject to a static and very high dynamic load. The rotor moves on a triangular orbit due to the high nonlinear bearing force, i.e. it largely follows the bearing contour. By taking the pad deformation into account, the orbit increases by about 15 % compared to that without deformations. These curves agree very well with the results of Desbordes et al. ([12], Figure 9), who were solving the Reynolds equation in each time step. This prooves that also a table look up method is able to predict the nonlinear vibration behaviour of a rotor supported in hydrodynamic bearings.

A more precise calculation would consider the 3D-Temperature distribution in the oil-film and in the bearing, the turbulent flow regime, time-dependent cavitation boundaries, the convective and local inertia forces, but would lead to excessive analysis time and such a calculation of trajectories is limited to exceptional cases. Therefore the

components of the transient bearing force $(So_D, \alpha_D, \beta_{ik}^*)$ are precalculated at certain grid points (grey crosses in Figure 2). These grid points are automatically distributed by the program ALP3T2Penhanced, so that nearly 99.99% of the possible shaft deflection is covered
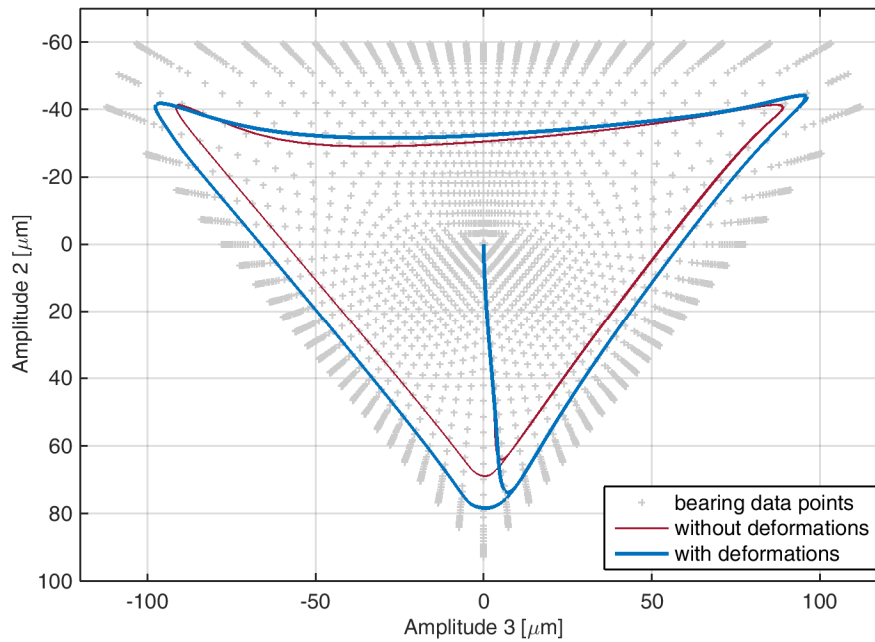
Figure 2: Journal centre orbit for a static load (30 kN) with a high unbalance force (50 kN) in 3-pad tilting pad bearing (D = 120 mm, B/D = 0.6, ψ = 1‰, 2 = vertical, 3 = horizontal)

3 Simulation Model

The structure of the rotor model for the exhaust turbocharger is shown in Figure 3. The rotor is pinned in semi-floating ring bearings. As the stiffness of the bearings is rather low, it can be assumed that the casing and the rings are rigid. The rotor is modelled in MADYN 2000 by using the Timoshenko beam theory and finite elements with 4th order Hermit polynomials to model the elastic and inertia properties of rotors including the gyroscopic effect. The semi-floating rings are modelled as concentrated masses which can only move in radial direction.
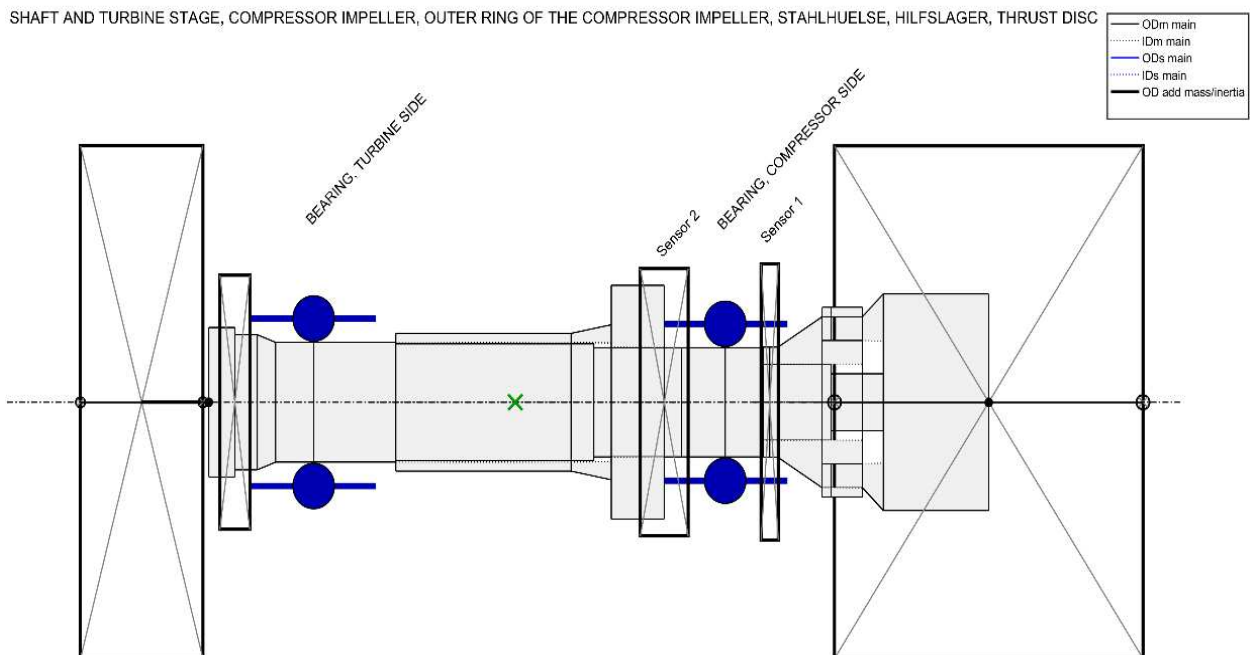
Figure 3: Model of exhaust turbocharger

The geometry and the clearance plot of the semi-floating ring bearings are shown in Figure 4. The inner oil film is modelled as a cylindrical three lobe pocket bearing while the outer oil film is modelled as a cylindrical squeeze-film damper with a deep hydrostatic groove. The bearing characteristics are previously calculated on defined grid points as mentioned before. The bearing characteristics are interpolated between these grid points during the simulation.
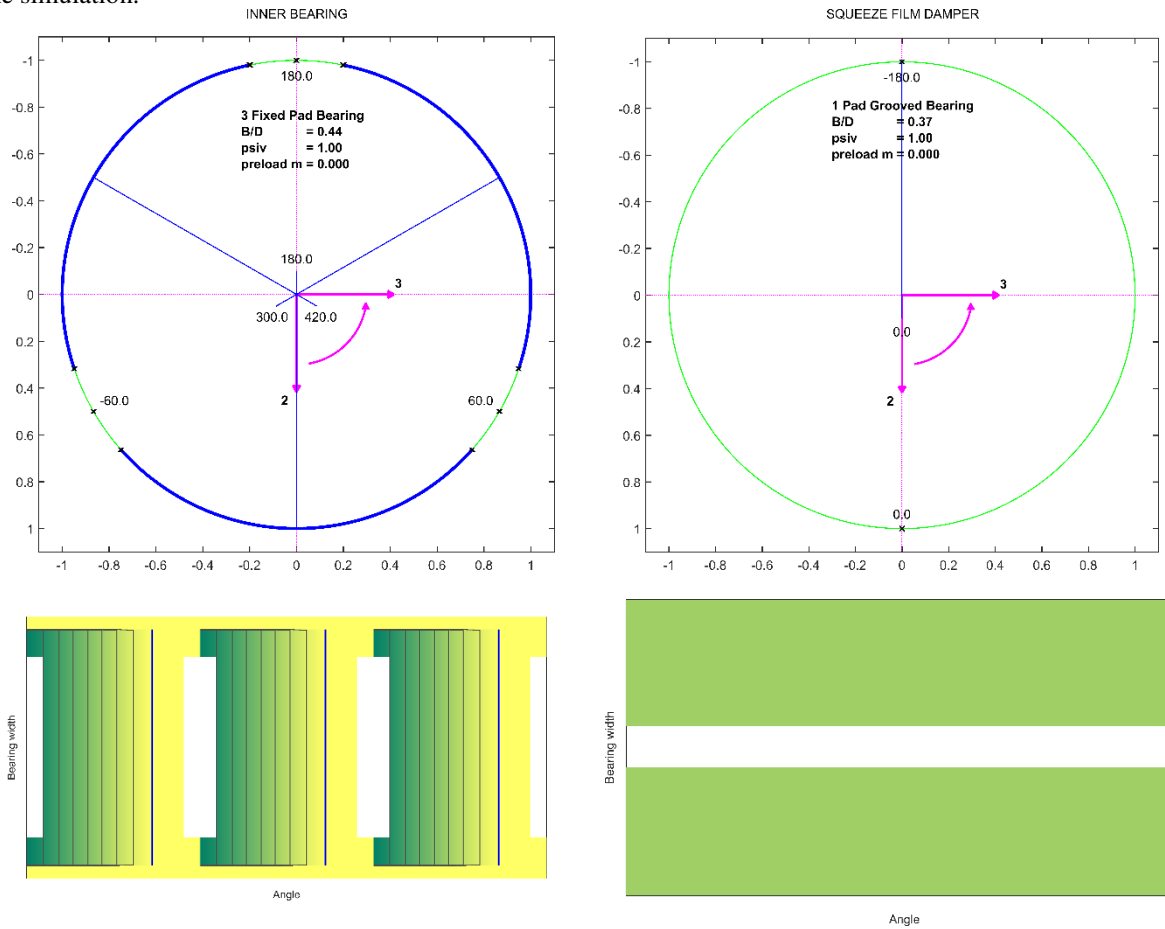
Figure 4: Geometry and clearance plot of semi floating ring bearings

During run-up the power loss in the inner oil film increases proportional with the square of the rotor speed, while the oil flow is proportional to the speed. Thus the mean temperature increases nearly proportional with the speed. This effect is implemented in MADYN 2000 by a DIN-like algorithm [2] taking into account the heat flow through the semi-floating ring. The calculated temperatures for shaft, ring and outer bearing are shown in Figure 5 (left). As expected, all temperatures increase nearly linearly with the speed. A certain deviation from linearity can be observed, which arises from the change of the bearing clearances of the inner and outer film (see Figure 5 right). As the clearance for the inner oil film increases slightly with the speed due to the thermal deformations the growth of the power loss is lower than quadratic with the speed.
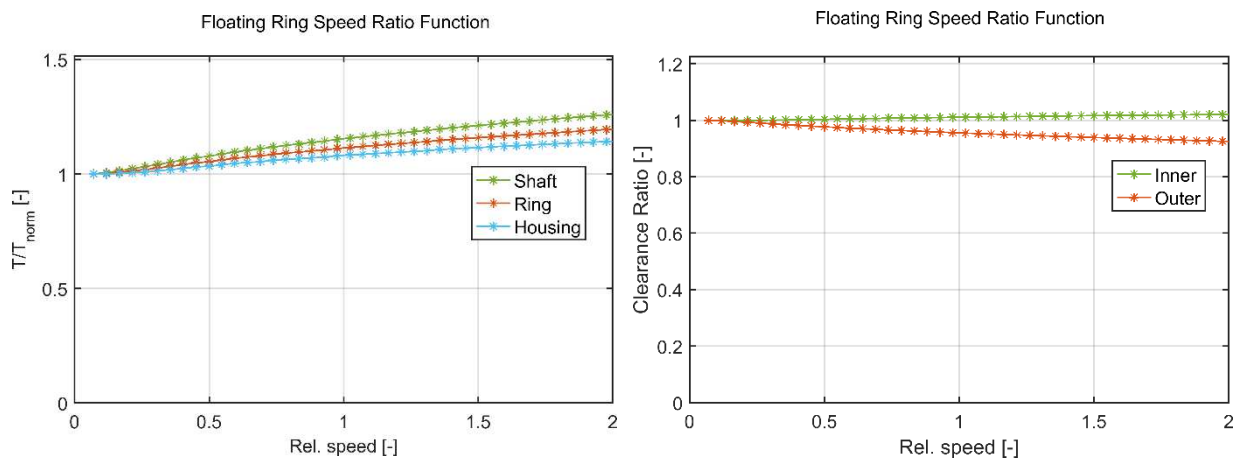
Figure 5: Calculated temperatures and changes of the bearing clearance

4 Calculation Results for a Squeeze-Film-Damper

For a turbocharger with two floating ring bearings with non-rotating rings the trajectories are plotted in Figure 6. The movement of the floating ring itself is shown in the right picture, while the relative shaft to ring vibration is in the left one. The calculation have been started for nominal speed with centred ring and shaft position. The bearing at "C-side" is statically nearly unloaded, while the other bearing has to carry the whole weight of the turbocharger. The shaft and the ring drop down directly after starting the calculation. The inner oil film produces immediately a film pressure due to the rotation of the shaft, whereas the ring must be accelerated to a certain velocity, so that the outer oil film can carry the mass of the ring and the shaft. As the vibration velocity of the ring is increased, the ring starts to centre itself. Sub-synchronous vibrations appear due to the low loading of the bearings.
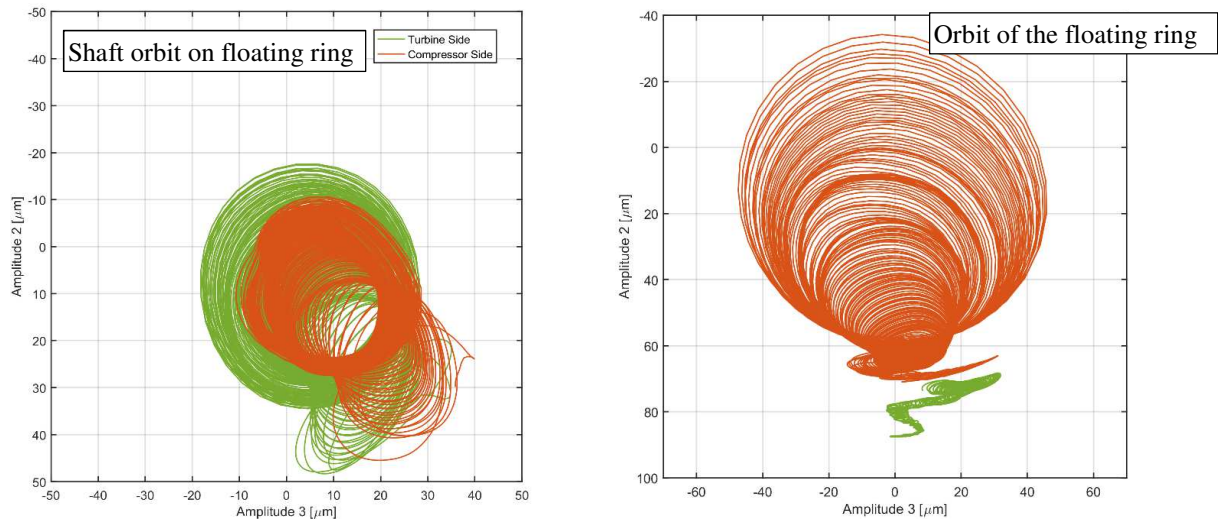
Figure 6: Orbit plots of the squeeze film ring and the shaft relative to the ring in a turbocharger

5 Comparison of Measured and Calculated Results

The measuring program consist of two bearing clearance combinations, two oil inlet temperatures and two unbalance cases. For the clearance combination maximum clearance inner and outer oil film (max/max) the comparisons are carried out for the two oil inlet temperatures and the two unbalance cases, while they are carried out for the clearance combination maximum clearance inner oil film and minimum clearance outer oil film (max/min) only for the high unbalance and both oil inlet temperatures.

5.1 Exhaust Turbo Charger with Minimum Clearance in the Outer Film, Small Unbalance

The first test was performed with the small unbalance. Figure 7 shows the measured and the calculated run-up in comparison. This test has been performed for the max/min clearance case with maximum oil inlet temperature.

The amplitudes of the synchronous vibration are very similar in the measurement and in the simulation. In the simulation the main sub-synchronous vibration starts at a slightly higher speed as in the measurement. The amplitude of the sub-synchronous vibration is at lower speeds appreciable higher than in the measurement. The maximum amplitude of this sub-synchronous has the same magnitude in the measurement and in the simulation. Also the 1st harmonic vibration is noticeable in the measurement and in the simulation.

In the simulation also combinations of the sub-synchronous and the synchronous or their harmonics are noticeable. These combinations were filtered out in the measurement.

5.2 Exhaust Turbo Charger with Maximum Clearance in the Outer Film, Small Unbalance

The second test was also performed with the small unbalance. Figure 8 shows the measured and the calculated run-up in comparison. This test has been performed for the max/max clearance case with nominal oil inlet temperature.

The amplitudes of the calculated synchronous vibration show good agreement with the measured ones. In this case only small portions of sub-synchronous vibrations with a relative frequency of about 0.3 can be observed in a relative speed range between 0.75 and 1. The occurrences of the sub-synchronous vibrations in the calculations depends on the acceleration time. For an acceleration time of 1 s no sub-synchronous vibrations can be observed in the relative speed range from 0.25 to 1.1. If the acceleration time is 5s, small portions of sub-synchronous vibrations can be observed.
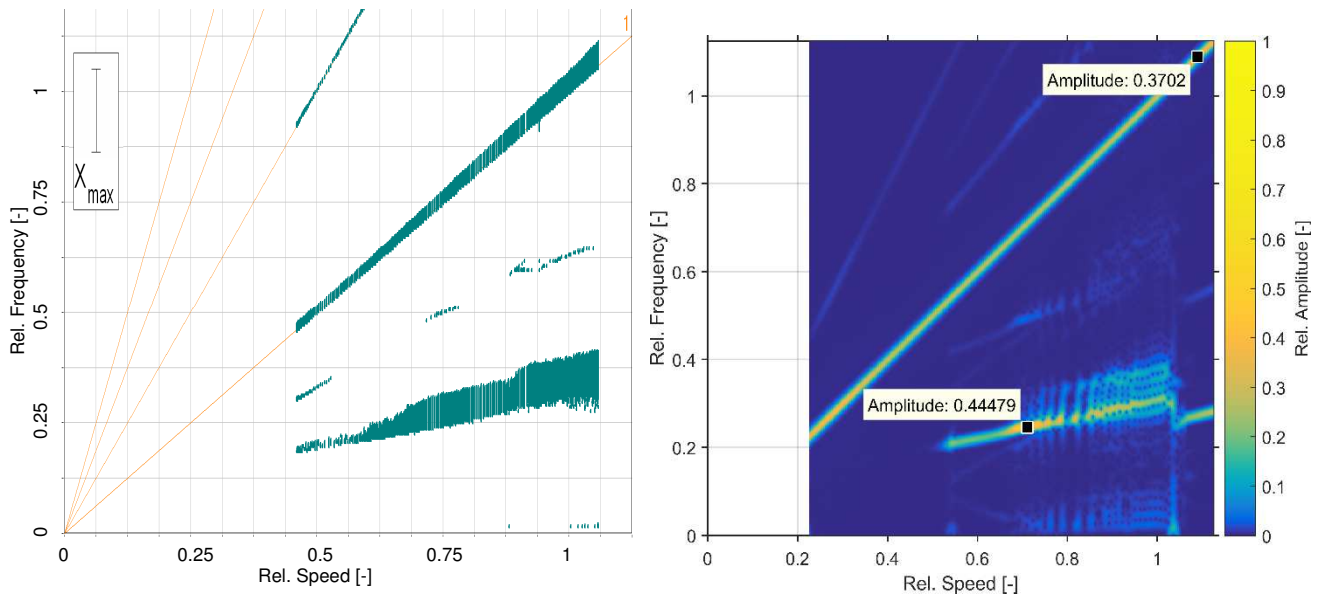
Figure 7: Spectrogram of run-up at sensor 1 (left measurement, right simulation)
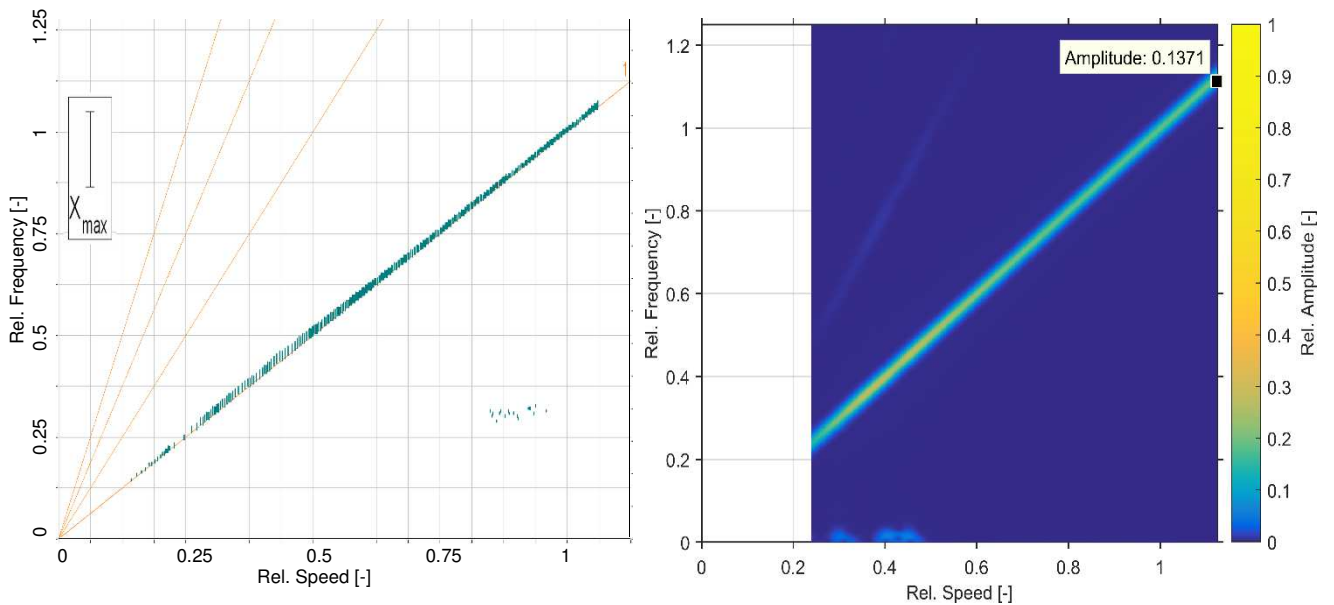
Figure 8: Spectrogram of run-up at sensor 1 (left measurement, right simulation)

5.3 Exhaust Turbo Charger with Maximum Clearance in the Outer Film, Big Unbalance

The third test was performed with the big unbalance. Figure 9 shows the measured and the calculated run-up in comparison. This test has been performed for the max/max clearance case with maximum oil inlet temperature.

The characteristics and the amplitudes of the calculated sub-synchronous vibration show good agreement with the measured results. This also applies for the synchronous vibration. In the measurement as well as in the calculation a frequency intersection of the sub-synchronous vibration can be observed at a relative speed of about 0.8. The onset of the sub-synchronous vibrations are different in that case, because the measurement itself was started at a relative speed of about 0.45.
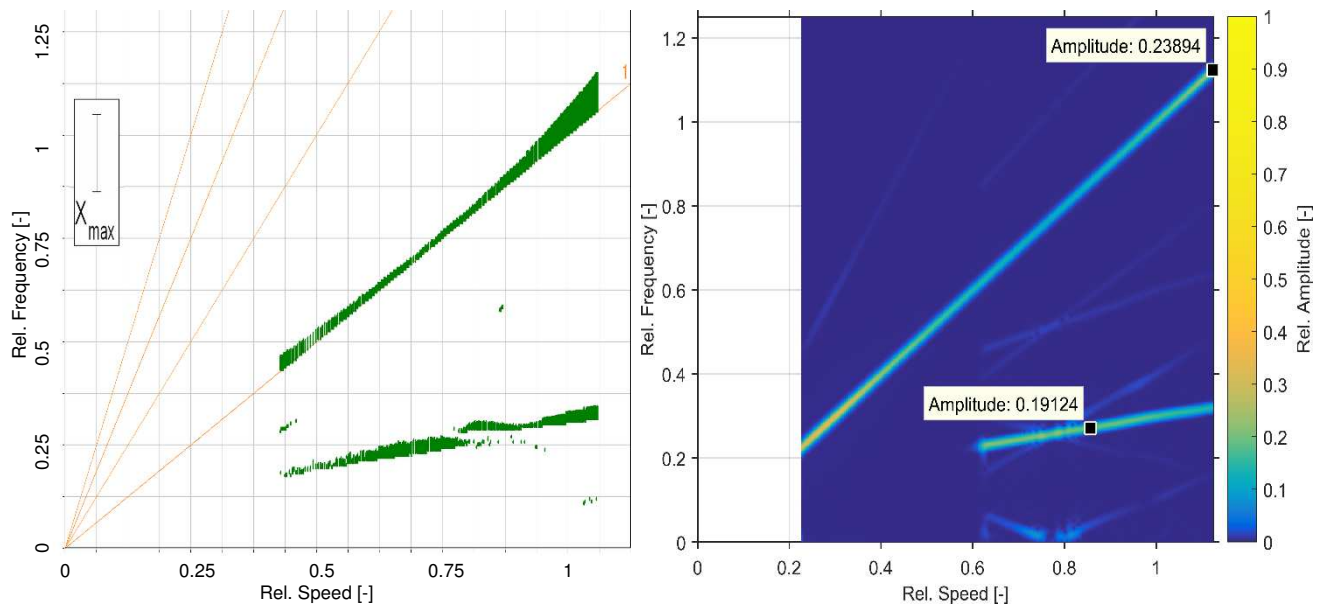
Figure 9: Spectrogram of run-up at sensor 1 (left measurement, right simulation)

6 Conclusion

By integrating the program ALP3T2Penhanced into the program-system MADYN 2000, the vibration behaviour of rotor – bearing – support systems can be accurately calculated in this case for a big turbocharger supported in semi-floating ring bearings. Analysing such systems reveals that the damping in the cavitation areas and the local inertia forces in the lubricating oil films can significantly change the non-linear vibration behaviour of such complex systems. For the present example with statically non-centred, non-rotating floating ring bearings, which act as squeeze film dampers, the important centring effect due to the dynamic load (actually creating load carrying capacity) can be clearly shown. The resulting synchronous as well as non-synchronous vibrations agree well with measured results regarding amplitude and frequency.

This proves, that the simplifications, which were used in order to allow an efficient analysis, did not compromise the quality of model.

References

[1] Holland, J., Berkowitz, B., Schwarze, H. (1991): Instationär belastete Gleitlager. *Tribologie und Schmie-rungstechnik* **39**, pp. 94-100.

[2] DIN 31657 (1996): *Hydrodynamische Radialgleitlager im stationären Betrieb. Berechnungsgrundlagen für Mehrflächen- und Kippsegmentlager*. Beuth, Berlin.

[3] Mittwollen, N., Rückert, A., Schmitz, A., Reinhardt, W.-D. (1991): Verbesserung der Berechnungsgrundlagen für schnelllaufende hochbelastete Mehrgleitflächen- und Radialkippsegmentlager. Abschlußbericht BMFT-Verbundprojekt „Gleitlageruntersuchungen" (Teilprojekt 03T0012A). TU Braunschweig.

[4] Meyer, A. (1987): *Äußere Lagerdämpfung für sehr hochtourige, gleitgelagerte Rotoren*. Dissertation U Karlsruhe.

[5] Schmied, J., Perucchi, M, Pradetto, J-C. (2007): Application of MADYN 2000 to rotordynamic problems of industrial machinery. IGTI, GT2007-27302.

[6] Fuchs, A. (2002): *Schnelllaufende Radialgleitlagerungen im instationären Betrieb*. Dissertation TU Braunschweig.

[7] Han, D. C. (1979): *Statische und dynamische Eigenschaften von Gleitlagern bei hohen Umfangsge-schwindigkeiten und bei Verkantung*. Dissertation U Karlsruhe.

[8] Peeken, H., Benner, J. (1985): Beeinträchtigung des Druckaufbaus in Gleitlagern durch Schmierstoffver-schäumung. *VDI-Bericht*. **549**, pp 371–397, VDI, Düsseldorf.

[9] Werner, H. K. (1986): *Schmierstoffe*. Deutsche Shell AG.

[10] Pinkus, O., Sternlicht, B. (1961): *Theory of Hydrodynamic Lubrication*. McGraw-Hill, New York, To-ronto, London.

[11] Falz, E. (1931): *Grundzüge der Schmiertechnik*. Springer, Berlin.

[12] Desbordes, H., Fillon, M., Chan Hew Wai, Frene, J. (1994); *Dynamic Analysis of Tilting-Pad Journal Bearing – Influence of Pad Deformations*. J. of Trib. **116**, pp. 621-628.